DOI:10.1190/tle40040302.1

Welcome to the latest installment of Geophysics Bright Spots. There are a number of interesting articles in the latest issue of Geophysics. Here is a list of what piqued the editors' interests.

Mechanical properties of grain contacts in unconsolidated sands

Unconsolidated sands are important for freshwater aquifers, hydrocarbon production, and CO_2 sequestration due to their high porosity and permeability. Understanding the acoustics of unconsolidated sands is required for the characterization of formations using ultrasonics, borehole acoustics, and seismic methods. Elastic wave propagation in unconsolidated sands is usually treated using idealized models of packings of identical elastic spheres. However, in real unconsolidated sands, the grains are neither spherical nor the same size. In "Mechanical properties of grain contacts in unconsolidated sands," Sayers investigates the elastic properties of unconsolidated sands using an extensive set of P- and S-velocity measurements and an approach based on the divergence theorem. Grain contacts are found to be more compliant under shear than under normal compression, and the ratio of normal-to-shear compliance decreases with decreasing confining pressure. This implies that shear compliance increases faster with decreasing confining pressure than normal compliance. This is important in understanding the role of shear in the failure of unconsolidated sands, such as in shallow-water flow, sanding, and failure around injectors, where change in stress is a function of the ratio of the normal-to-shear compliance ratio of the grain contacts.

Efficient frequency-domain FWI

Long-offset sparse ocean-bottom node (OBN) acquisitions are emerging as the way forward for deep offshore exploration. In this framework, frequency-domain full-waveform inversion (FD-FWI) has advantages in building high-resolution subsurface models from a compact volume of data. Frequency-domain seismic modeling is a challenge because it requires solving linear systems with multiple right-hand sides (sources) with either direct or iterative methods. Direct methods should be preferred to process multiple sources efficiently. However, the lower-upper (LU) decomposition of the impedance matrix remains expensive. Another issue is the nonlinearity of FWI generated by cycle skipping. Contrast-source inversion (CSI) was proposed a decade ago as an efficient FD-FWI with a direct solver. The idea is to reparametrize the wave equation with a scattered-field formulation to perform one LU factorization per frequency during inversion iterations. The wavefield reconstruction inversion based on augmented Lagrangian (iteratively refined wavefield reconstruction inversion [IR-WRI]) has been proposed to extend the search space of FD-FWI by solving the wave equation with data assimilation. In "On efficient frequency-domain full-waveform inversion with extended search space," Aghamiry et al. review connections between CSI and IR-WRI before proposing a new approach to FD-FWI that combines advantages of both methods. Application on 2D complex benchmarks shows that the new method reconstructs the models as accurately as classical IR-WRI while reducing the number of LU factorizations with a

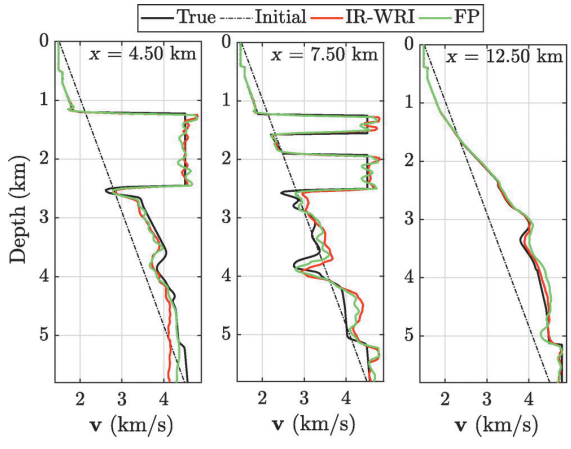

Figure 1. (Figure 16 from Aghamiry et al.) The 2004 BP salt test. Direct comparisons along the logs at $x = 4.50$ km (left), $x = 7.50$ km (center), and $x = 12.50$ km (right) between the true model (black), initial model (dashed line), bound-constrained Tikhonov-Total variation regularized IR-WRI (red), and efficient fixed-point-based IR-WRI (green).

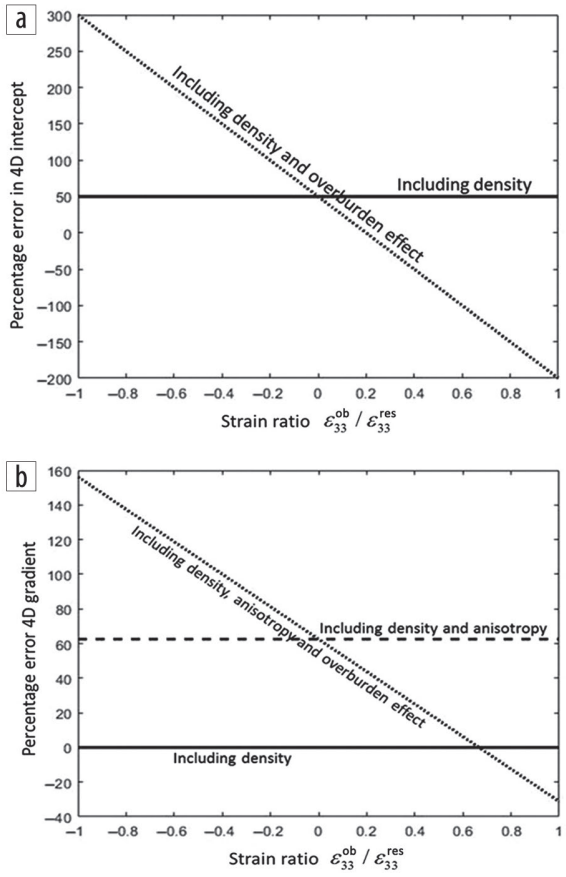

Figure 2. (Figure 2 from MacBeth and Bachkheti) Percentage error in the 4D intercept and 4D gradient terms due to neglecting the density term, anisotropy in the reservoir, and effect of the overburden. Error is defined as a function of the ratio of vertical strain in the overburden to vertical strain in the reservoir $\varepsilon^{ob}/\varepsilon^{res}$.

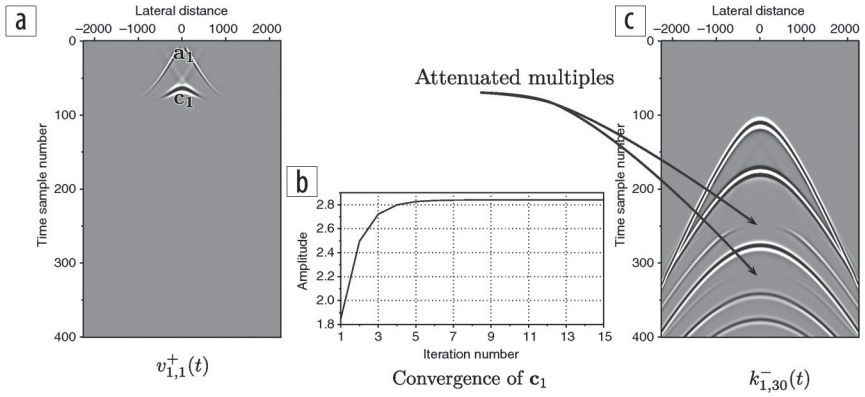

Figure 3. (Figure 6 from Thorbecke et al.) Using only the primary reflections of the first and second reflector, a new event (c_1) is created. This new event annihilates all internal multiples between the first two reflectors from the shot record.

fixed-point algorithm (Figure 3). A theoretical complexity analysis inspired by a real 3D FD-FWI case study suggests that the proposed algorithm should reduce the cost of IR-WRI by one order of magnitude for 3D sparse OBN surveys.

Determination of the time-dependent moment tensor

Determination of the source mechanism is crucial for many applications. For example, in geothermal and hydrocarbon reservoirs, it may reveal the likelihood of events being of natural or anthropogenic origin and increase the understanding of subsurface physical processes. To observe the subsurface, it is crucial that the employed tools rely on as few a priori assumptions about the seismic events as possible. In "Determination of the time-dependent moment tensor using time reverse imaging," Finger and Saenger present an approach to determine hypocenter locations and time-dependent six-component moment tensors without a priori knowledge. The approach backpropagates the time-reversed wavefield recorded at the surface until it focuses at the source location. Imaging conditions are used to find source locations, and the stress tensor is recorded at the source locations. The stress tensor can be related to the moment tensor and provides a full characterization of the seismic event. Subsequently, common parameters such as fault-plane orientations and origin times can be derived from the moment tensors. Because the method does not rely on the identification of phases in the recorded seismic traces, it is well suited for data with low signal-to-noise ratio. This holds true for the determination of moment tensors and provides a way to locate and characterize microseismic events in any application.

Geomechanical correction for time-lapse AVO

In "A geomechanical correction for time-lapse amplitude variation with offset," MacBeth and Bachkheti explore the affect of changes in stress/strain in the overburden and reservoir on time-lapse amplitude variation with offset (AVO) inversion. MacBeth notes that "the inspiration for this paper arose from a relaxed discussion with Jorg Herwanger in a bar during a geophysical conference. Jorg and I were reflecting on the current use of AVO in 4D quantitative interpretation and the role of geomechanics. In a 4D context, AVO was often used to separate pressure and saturation signals. Jorg felt that geomechanics would make a big difference and add value to our current understanding."

The authors determine that there are three contributions that must be included in the AVO equations: a density term in the reservoir, seismic anisotropy generated by reservoir deformations, and the impact of changing overburden properties. They find the 4D AVO behavior to be controlled by three *R*-factors that relate to time-lapse variations in P- and S-wave velocities. Their numerical computations indicate that the error in accounting for the anisotropy contribution to the P-P reflectivity can be as high as 50%–300% for the 4D zero-offset intercept and 62%–155% for the 4D gradient. In most applications, time-lapse anisotropy in the reservoir and overburden cannot be neglected when estimating pressure changes using 4D AVO.

Implementation of the MME algorithm

The Marchenko multiple elimination (MME) algorithm uses primary reflections to estimate multiple reflections between reflectors. The method uses reflection data as the only input. The output is the reflection data without internal multiples. In "Implementation of the Marchenko multiple elimination algorithm," Thorbecke et al. explain the algorithm in easy-to-follow steps and guide the reader on how internal multiples are eliminated in a shot record by using the shot record itself. The MME method is an iterative process that consists of convolutions and correlations between the reflection data of all available shots and the selected shot record. The convolutions and correlations are applied alternately. Following each convolution or correlation, a constant time truncation sets all times to zero after a preselected time instant. This time-truncated result becomes the input for the next correlation or convolution. The algorithm typically converges in 10–15 iterations and creates new events — one for each primary reflector in the time window above the time truncation. These events annihilate all internal multiples between reflectors in the time window. Once a first-order internal multiple is eliminated, the whole train of multiples associated with the first-order multiple are eliminated as well. The authors made the algorithm and software available through GitHUB and the SEG software portal. TLE

References

Aghamiry, H., A. Gholami, and S. Operto, 2021, On efficient frequency-domain full-waveform inversion with extended search space: Geophysics, **86**, no. 2, https://doi.org/10.1190/geo2020-0478.1.

Finger, C., and E. H. Saenger, 2021, Determination of the time-dependent moment tensor using time reverse imaging: Geophysics, **86**, no. 2, KS63–KS77, https://doi.org/10.1190/geo2020-0348.1.

MacBeth, C., and S. Bachkheti, 2021, A geomechanical correction for time-lapse amplitude variation with offset: Geophysics, **86**, no. 2, M29–M40, https://doi.org/10.1190/geo2020-0398.1.

Sayers, C., 2021, Mechanical properties of grain contacts in unconsolidated sands: Geophysics, **86**, no. 2, MR95–MR103, https://doi.org/10.1190/geo2020-0479.1.

Thorbecke, J., L. Zhang, K. Wapenaar, and E. Slob, 2021, Implementation of the Marchenko multiple elimination algorithm: Geophysics, **86**, no. 2, F9–F23, https://doi.org/10.1190/geo2020-0196.1.